Geophys. J. Int. (1997) **128**, 689–700

Inversion of seismic attributes for velocity and attenuation structure

Robert L. Nowack and Michael P. Matheney

Department of Earth and Atmospheric Sciences, Purdue University, West Lafayette, IN 47907. *E-mail: nowack@geo.purdue.edu*

Accepted 1996 November 12. Received 1996 November 6; in original form 1996 May 20

SUMMARY

We have developed an inversion formulation for velocity and attenuation structure using seismic attributes, including envelope amplitude, instantaneous frequency and arrival times of selected seismic phases. We refer to this approach as AFT inversion for amplitude, (instantaneous) frequency and time. Complex trace analysis is used to extract the different seismic attributes. The instantaneous frequency data are converted to t^* using a matching procedure that approximately removes the effects of the source spectra. To invert for structure, ray-perturbation methods are used to compute the sensitivity of the seismic attributes to variations in the model. An iterative inversion procedure is then performed from smooth to less smooth models that progressively incorporates the shorter-wavelength components of the model. To illustrate the method, seismic attributes are extracted from seismic-refraction data of the Ouachita PASSCAL experiment and used to invert for shallow crustal velocity and attenuation structure. Although amplitude data are sensitive to model roughness, the inverted velocity and attenuation models were required by the data to maintain a relatively smooth character. The amplitude and t^* data were needed, along with the traveltimes, at each step of the inversion in order to fit all the seismic attributes at the final iteration.

Key words: inversion, seismic refraction, seismic tomography.

INTRODUCTION

We have developed an inversion formulation for velocity and attenuation structure using seismic attributes. We refer to this as AFT inversion for amplitude, instantaneous frequency and traveltime attributes. This approach is an alternative to the direct inversion of seismic wavefield data, which can be highly non-linear. It also incorporates more of the seismic data than inversion using just traveltimes. The extraction of seismic attributes is performed by complex trace analysis; however, a more general wavelet analysis could also be used. The instantaneous frequency data are converted to t^* by a matching procedure that approximately removes the effects of the source spectra (Matheney & Nowack 1995).

To invert for structure, ray-perturbation methods are used to compute the sensitivity of each attribute to changes in the model. An iterative inversion procedure from smooth models to less smooth models is then performed in order to progressively incorporate the shorter-wavelength features of the model. When inverting seismic attributes, such as amplitudes and instantaneous frequencies, both velocity and attenuation structure must be included. To illustrate the AFT inversion for laterally varying structure, seismic attributes extracted from refraction data recorded during the Ouachita PASSCAL experiment are used to invert for shallow crustal velocity and attenuation structure.

EXTRACTION OF SEISMIC ATTRIBUTES

The extraction of the seismic attributes can be performed using complex trace analysis (Taner, Koehler & Sheriff 1979), as well as by more general wavelet analysis (Daubechies 1992). The approach followed here is to use complex trace analysis to construct the analytic signal from the seismic trace. From the analytic signal, the envelope and instantaneous frequency can be determined where the resulting instantaneous frequencies are not generally equivalent to spectral frequencies (Cohen 1995).

The analytic signal can be written as

$$z(t) = y(t) + i\tilde{y}(t), \tag{1}$$

where $\tilde{y}(t)$ is the Hilbert transform of $y(t)$. Alternatively, $z(t)$ can be obtained from the positive frequencies of the spectrum of $y(t)$. The signal envelope is then

$$a(t) = [y^2(t) + \tilde{y}^2(t)]^{1/2}, \tag{2}$$

and the instantaneous frequency can be written

$$f_I(t) = \frac{1}{2\pi} \frac{y(t)\dfrac{d\tilde{y}(t)}{dt} - \tilde{y}(t)\dfrac{dy(t)}{dt}}{a^2(t) + \varepsilon^2}, \tag{3}$$

where ε^2 is a small damping used to stabilize the instantaneous frequency when the envelope gets small (Matheney & Nowack

1995). A weighted average of the instantaneous frequency over time is also performed to provide further smoothing of the estimate. An additional feature found to be useful for the estimate of instantaneous frequencies is the use of filtering to remove possible bias from seismic noise. Fig. 1 shows an example of the complex envelope and instantaneous frequency determined from an observed seismic trace. The phase times are extracted from either the onset time or peak amplitude of the envelope of selected seismic phases. In this study, the phase times of first-arrival onsets are determined interactively on the computer. The envelope peak amplitude and instantaneous frequencies are then extracted for the selected phase.

In order to obtain values of the attenuation factor, t^*, a matching procedure of the instantaneous frequencies between the observed data and a reference pulse is peformed (Matheney & Nowack 1995). In this approach, an attenuated reference pulse is written in the form

$$p(x, t) = p(x_{\text{ref}}, t)^* \text{IFT}[\exp[i\omega(T + \alpha t^*)]], \quad (4)$$

where $p(x_{\text{ref}}, t)$ is a near-source reference pulse, T is the traveltime, $t^* = \int uQ^{-1}\, ds$ is the attenuation factor, $u(\mathbf{x})$ is the slowness or inverse velocity and $Q^{-1}(\mathbf{x})$ is the inverse of the quality factor. IFT is an inverse Fourier transform and * indicates convolution. For a causal attenuation operator, $\alpha = -\ln(\omega/\omega_r)/\pi + i/2$, where ω_r is the frequency to which the attenuation model is referenced (Aki & Richards 1980).

In order to estimate t^* between a trace and a near-offset reference pulse, the instantaneous frequency is first determined from complex trace analysis of the individual traces. An inverse problem for t^* is then formulated and solved iteratively to find the relative attenuation factor $t^*(x; x_{\text{ref}}, x_0)$ between the observed pulse at x and a near-offset reference pulse at x_{ref}. The matching of instantaneous frequency data to determine t^* has the advantage of incorporating the reference pulse spectrum into the estimation of t^*, and was found to be more stable than the use of spectral ratios (Matheney & Nowack 1995).

An alternative seismic attribute is the polarization angle for P waves and this has been used along with traveltime for inversion by Hu & Menke (1992). However, the use of polarization angles requires three-component data. In the approach followed here, polarization angles are not directly incorporated since only single-component data are assumed. Nonetheless, ray-angle information is indirectly incorporated in the amplitude data.

An example of an observed crustal seismic gather is shown in Fig. 2. Although the amplitudes are normalized for plotting purposes, estimates of envelope amplitudes and instantaneous frequencies can be obtained from the first-arrival pulses of the gather. From the instantaneous frequencies, estimates of relative t^* can be obtained using the matching procedure above. Examples of seismic attributes estimated from an observed seismic gather from the Ouachita PASSCAL experiment are shown in Fig. 3 (squares), along with the smoothed and interpolated values used for inversion (dots). In Figs 3(b) and (c), the relative amplitudes and t^* values are shown.

RAY-PERTURBATION ANALYSIS

Ray-perturbation methods are used to perform sensitivity analysis of the seismic attributes to variations in the model.

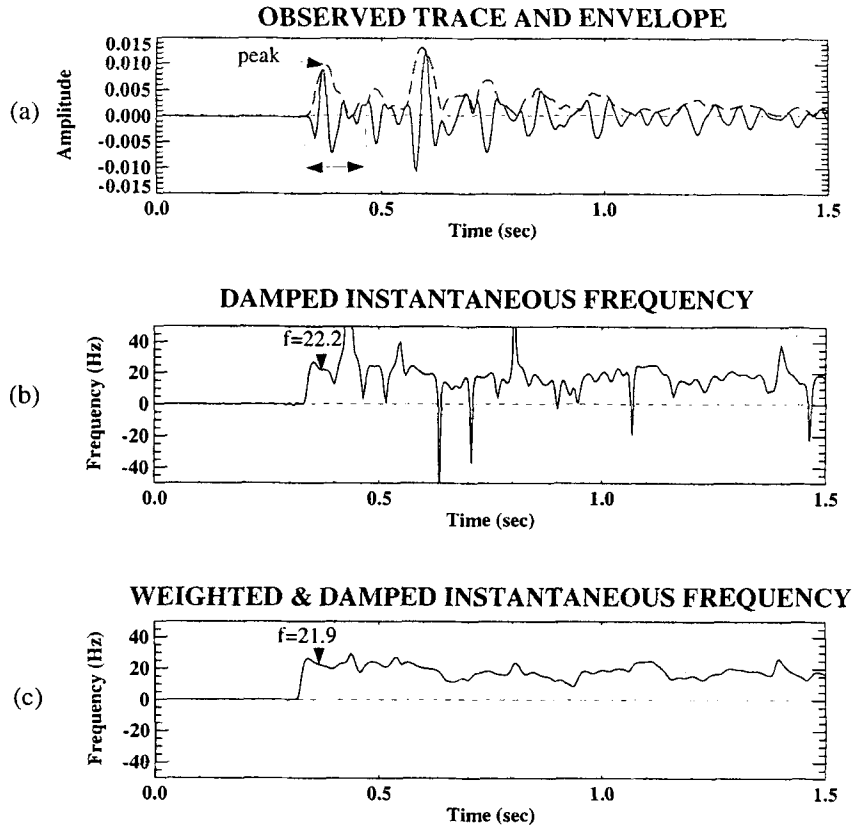

Figure 1. (a) An observed seismic trace and its complex envelope. (b) Damped instantaneous frequency of the seismic trace in (a). (c) Weighted and damped instantaneous frequency. For the initial peak of the first arrival envelope, the instantaneous frequency is indicated.

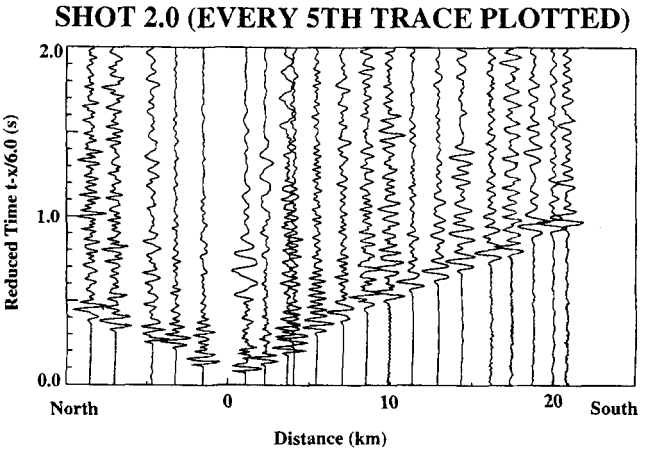

Figure 2. Observed crustal seismic gather from the Ouachita PASSCAL refraction experiment displaying pulse broadening of the first arrivals.

For an initially homogeneous medium, ray-perturbation results were obtained by Keller (1962), Moore (1980, 1991) and Norton & Linzer (1982). Farra & Madariaga (1987) applied ray-perturbation theory to compute traveltimes and amplitudes in slightly perturbed media for a laterally varying initial medium. An application of ray-perturbation theory to the inversion of traveltimes and amplitudes was given by Nowack & Lutter (1988). To this approach, interfaces were incorporated by Farra, Virieux & Madariaga (1989) and Nowack & Lyslo (1989).

Sneider & Sambridge (1992) investigated higher-order traveltime perturbations using a Lagrangian approach and showed that second-order traveltime perturbations could be obtained from first-order ray-perturbation analysis. The second-order traveltime perturbation analysis was developed by Snieder & Spencer (1993) and Snieder & Sambridge (1993) for general ray coordinates, while Snieder & Aldridge (1995) extended the analysis to higher-order phase-time perturbations.

In order to invert for seismic attributes, perturbation analysis of these attributes to medium variations is required. As a first step, the linearized ray equations in Cartesian coordinates can be written

$$\begin{bmatrix} \delta\dot{x}_i \\ \delta\dot{p}_i \end{bmatrix} = \begin{bmatrix} 0 & u^{-1}(\delta_{ij} - \dot{x}_i\dot{x}_j) \\ \dfrac{\partial^2 u}{\partial x_i \partial x_j} & 0 \end{bmatrix} \begin{bmatrix} \delta x_j \\ \delta p_j \end{bmatrix} + \begin{bmatrix} 0 \\ R_i^1 + R_i^B \end{bmatrix} + \delta h \begin{bmatrix} \dot{x}_i \\ \dfrac{\partial u}{\partial x_i} \end{bmatrix}, \tag{5}$$

where δx_i and δp_i are the perturbations of position and slowness vector along the ray, δ_{ij} is the Kronecker delta symbol, δu is the slowness perturbation, and $h = (1 + \delta h)$ is the ray-stretch factor (Farra, Madariaga & Virieux 1994). The dots refer to derivatives with respect to distance along the ray. $R_i^1 = \partial\delta u/\partial x_i$ is the term due to the slowness perturbation and

$$R_i^B = \frac{\partial u}{\partial x_i} - \frac{d(u\dot{x}_i)}{ds}$$

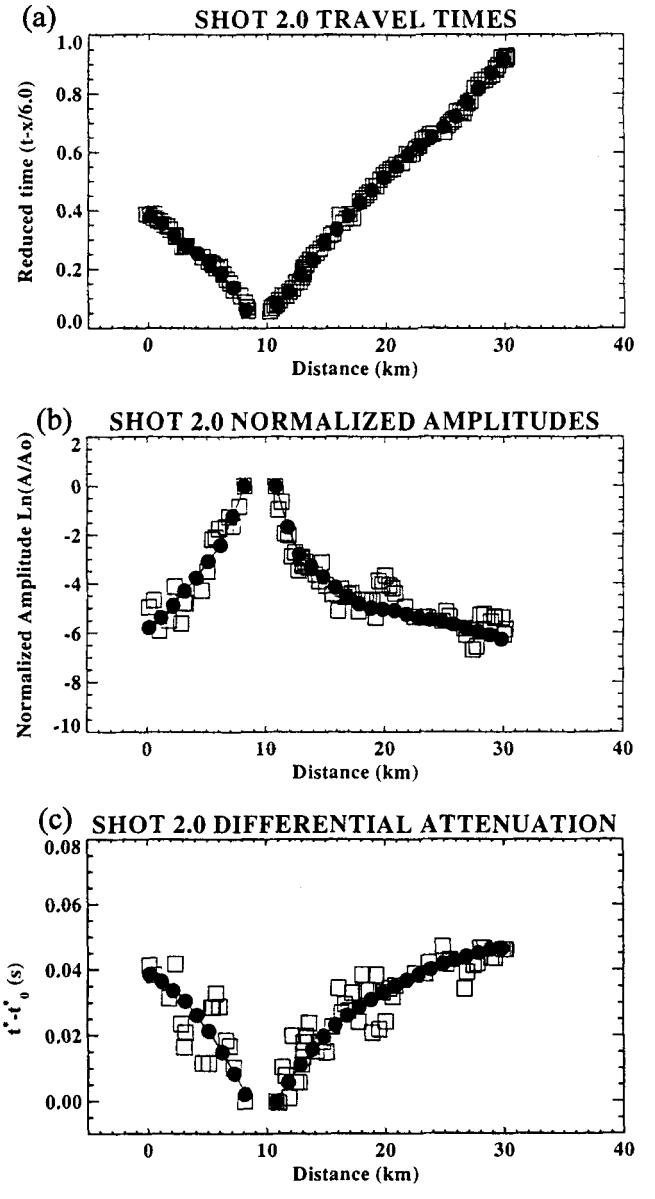

Figure 3. Observed and interpolated seismic attribute values from the gather in Fig. 2. (a) Observed and interpolated traveltimes. (b) Observed and interpolated ln (A/A_0), where A_0 is the amplitude at a near-offset reference distance. (c) Observed and interpolated relative t^* values between the observed data and a nearby reference station. For each case, the squares are the raw data and the circles are the smoothed data.

is an initial ray-bending term. The solution of (5) can be written as

$$\begin{bmatrix} \delta x_i(\tau) \\ \delta p_i(\tau) \end{bmatrix} = P(\tau, 0) \begin{bmatrix} \delta x_i(0) \\ \delta p_i(0) \end{bmatrix} + \int_0^\tau P(\tau, \tau') B(\tau')\, d\tau', \tag{6}$$

where $B(\tau)$ includes the last two source terms in (5) and $P(\tau, \tau')$ is the linearized ray propagator in the initial medium. The values $\delta x_i(0)$, $\delta p_i(0)$ and δh are specified to satisfy the boundary conditions on the ray. As an alternative, the linearized ray equations can be written in ray-centred coordinates, which reduces the linearized system from six variables to four, but requires additional analysis at interfaces and boundaries (Farra

& Madariaga 1987). In either case, once the perturbed ray is determined, changes in the seismic attributes computed along it can be determined.

The first-order traveltime or phase perturbation can be obtained from Fermat's principle as an integration of the change in the slowness along the unperturbed ray path. Thus

$$\delta T_1 = \int_0^{s_0} \delta u ds_0 + u_0 \dot{x}_i \delta x_i |_0^{s_0}, \tag{7}$$

where the last term is a boundary term related to the change in the ray endpoint positions (Aki & Richards 1980). The use of first-order perturbations in traveltime tomography allows for significant computational savings as compared to more direct calculations of traveltime sensitivity. As a result, most recent tomographic inversion methods use first-order analysis, with higher-order terms included in the inversion via iteration.

The second-order traveltime perturbation has been obtained by Snieder & Sambridge (1993) and can be written

$$\delta T_2 = \frac{1}{2} \int_0^{s_0} \delta x_i \{R_i^{1S} + R_i^B\}\, ds_0 + \text{B.T.}, \tag{8}$$

where B.T. represents the endpoint boundary terms,

$$R_i^{1S} = \frac{\partial \delta u}{\partial x_i} - \frac{d}{ds_0}[\delta u \dot{x}_i]$$

is the slowness perturbation term, and

$$R_i^B = \frac{\partial u_0}{\partial x_i} - \frac{d}{ds_0}[u_0 \dot{x}_i]$$

is the ray-bending term used when the initial trajectory is not a true ray [see eq. (45) of Snieder & Sambridge (1993)].

As an example, Fig. 4 shows the variation in seismic attributes caused by the perturbation of a splined velocity node. Fig. 4(a) shows the reference rays used for a test of the ray-perturbation analysis. The reference model is 1-D and smoothly varying with depth. The horizontal node spacing is 10 km and the vertical node spacing is 1.5 km. The perturbed traveltimes for a smoothly perturbed velocity node located at a distance of 40 km and a depth of 1.5 km are shown in Fig. 4(b). The velocity perturbation of that node is $-0.04\ \text{km s}^{-1}$ and is spline interpolated similar to the reference model. The solid

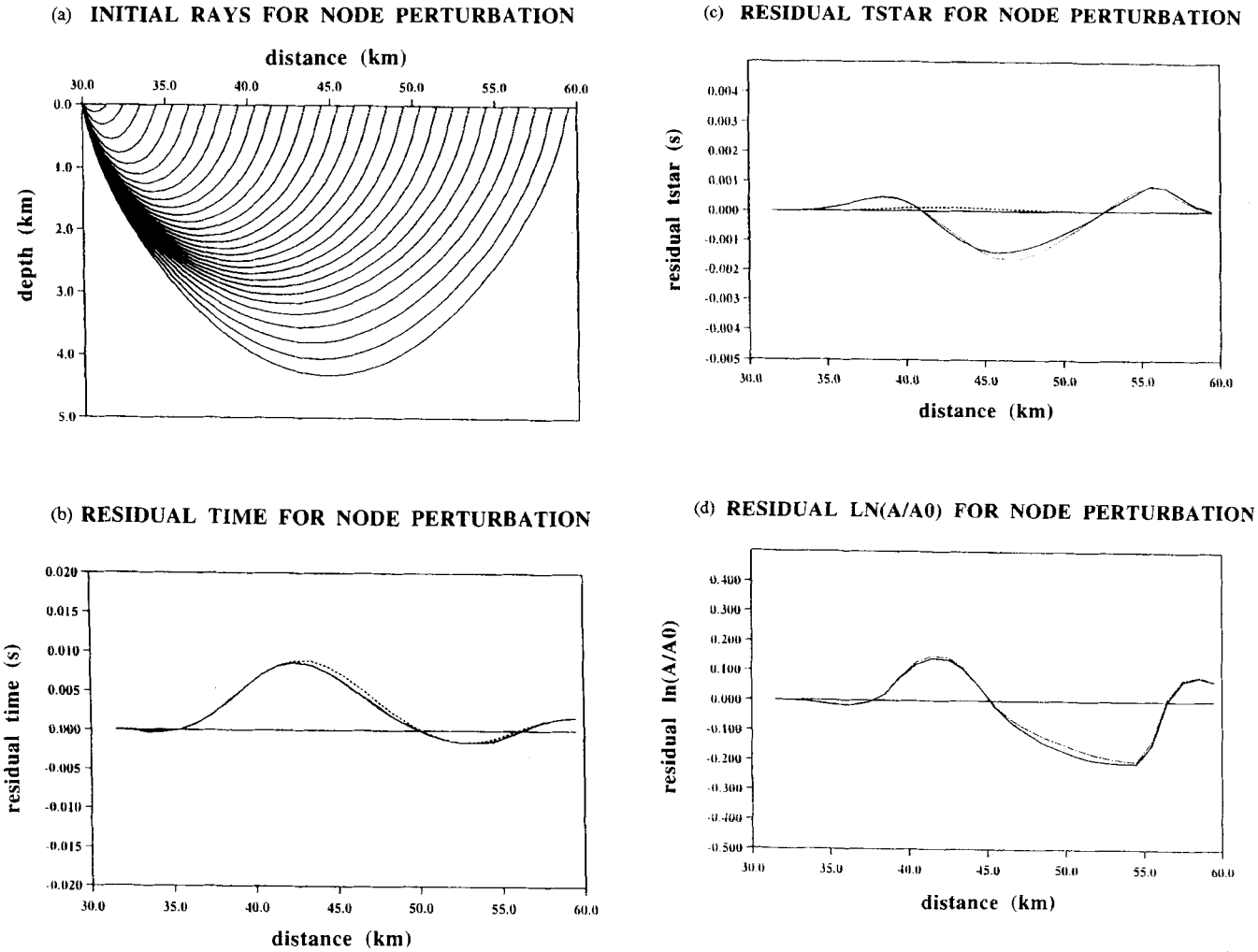

Figure 4. (a) An unperturbed ray framework used for the test of ray perturbations. The location of the perturbed node is centred at 40 km and a depth of 1.5 km. (b) Perturbed traveltimes. The solid curve is the residual times from direct ray tracing. The dashed line is from first-order and the dotted line from second-order ray tracing. The dotted line nearly coincides with the solid line. (c) Perturbed t^* values. The solid curved line is again from direct ray tracing. The dashed line is from an integration along the real reference ray. The dotted line is from the complete first-order term, including ray bending. (d) Perturbation of the natural log of the amplitudes, where the solid curve line is from direct ray tracing. The dash–dot line is the first-order term from ray perturbation analysis.

curved line in Fig. 4(b) shows the residual traveltimes from direct ray tracing in the perturbed and reference media. The dashed line is obtained from first-order traveltime perturbation analysis and the dotted line is from second-order traveltime analysis with ray bending. As shown in Fig. 4(b), the resulting second-order term (dotted) almost exactly overlies the curve from direct ray tracing (solid).

For the calculation of ray theoretical amplitudes, the dynamic, or paraxial ray equations are often used (Popov & Pšenčík 1978; Červený & Hron 1980). The dynamic ray equations have also been applied to more general wavefield calculations, such as Gaussian beam summation and Maslov methods (Červený, Popov & Pšenčík 1982; Chapman & Drummond 1982; Nowack & Aki 1984; Červený 1985). To include ray amplitudes within an inversion, the sensitivity of geometric amplitudes to changes in the model must be obtained. Nowack & Lyslo (1989) used ray-perturbation methods to obtain the perturbed ray amplitudes, including geometric spreading as well as transmissions and reflections at interfaces and the free surface. Fig. 4(d) shows the result of a velocity node perturbation on the vertical component amplitudes. The solid line shows the difference in ln amplitudes by the direct computations of the amplitudes in the perturbed and reference media. The dash–dot line is the residual ln amplitudes based on a first-order ray perturbation.

For realistic earth models, observed seismic amplitudes are also affected by attenuation. Anelastic calculations for slightly attenuating media can be obtained by a continuation of the elastic-wave solutions. For an effectively constant Q with frequency, to first-order an attenuated pulse can be written for positive frequencies as

$$p(x,\omega) = S(\omega)\exp[i\omega(T - \ln(\omega/\omega_r)t^*/\pi)]\exp[-\omega t^*/2], \quad (9)$$

where $T = \int u(x,\omega_r)\,ds$ is the traveltime along the ray, t^* is an attenuation factor equal to $\int u(x,\omega_r)Q^{-1}(x)\,ds$, and $S(\omega)$ is the initial pulse spectrum (Aki & Richards 1980).

Using first-order attenuation models, T and t^* are often computed along nearby real rays instead of the true complex rays for the attenuative media. As an alternative, a complex slowness perturbation from a slightly anelastic medium can be performed. The linearized ray equations of (5) can then be used to compute the ray perturbations from forcing terms that now depend on the complex slowness perturbation. The resulting perturbed rays in the anelastic medium will in general be complex. Complex phase-time perturbations are then computed as in the real case, except with a complex ray perturbation as well as a complex slowness perturbation. For amplitudes, complex reflection coefficients and complex geometric spreading also need to be included. As an example, Zhu & Chun (1994) used complex rays to include finite-ray effects by introducing a slightly perturbed complex slowness.

In the first-order linearized approach used here, attenuation is incorporated by computing t^* and the geometric spreading along a nearby real elastic ray. For this case, the first-order t^* perturbation to variations in the medium can be written

$$\delta t^* = \int [\delta u Q_0^{-1} + u_0 \delta Q^{-1}]\,ds_0 + \delta x_i u_0 Q_0^{-1}\dot{x}_i|_0^{s_0} + \int \delta x_i u_0 \left[\frac{\partial Q_0^{-1}}{\partial x_i} - \dot{x}_i \frac{dQ_0^{-1}}{ds}\right] ds_0, \quad (10)$$

where u_0 and Q_0^{-1} are the reference slowness and attenuation and δu and δQ^{-1} are the perturbations. Only the $\int u_0 \delta Q^{-1}\,ds_0$ term is non-zero if the starting model is elastic, with $Q_0^{-1} = 0$. When Q_0^{-1} is not equal to zero, all terms can contribute. In this case, the initial and final real trajectories are not true rays in the anelastic medium, and the last term on the right side of (10) can be considered a second-order term. However, this term is first-order with respect to the slowness perturbation through the variation in the ray position δx_i, and must be included in any first-order analysis of t^*.

As an example, Fig. 4(c) shows the effects of a velocity node perturbation on the t^* attenuation factor. The residual t^* values obtained from direct calculation are shown by the solid curved line. The dashed line results from a perturbation along a nearby real reference ray. The perturbed values of t^* taking into account the ray perturbation are shown by the dotted line in Fig. 4(c). Since both the velocity and attenuation models are generally unknown, a ray perturbation needs to be accounted for when computing first-order sensitivity of t^* along real rays.

TOMOGRAPHIC INVERSION OF SEISMIC ATTRIBUTES

After the seismic attributes have been extracted from the seismic data, an inversion of these attributes for velocity and attenuation structure can be performed. A linearized relation between variations in the slowness and inverse-Q model parameters, δu and δQ^{-1}, and the attribute residuals can be written

$$\begin{bmatrix} \delta T_R \\ \delta t^* \\ \delta \ln A \end{bmatrix} = \begin{bmatrix} \partial T_R/\partial u & \partial T_R/\partial Q^{-1} \\ \partial t^*/\partial u & \partial t^*/\partial Q^{-1} \\ \partial \ln A/\partial u & \partial \ln A/\partial Q^{-1} \end{bmatrix} \begin{bmatrix} \delta u \\ \delta Q^{-1} \end{bmatrix}, \quad (11)$$

where T_R is the complete real part of the traveltime including dispersion from the attenuation model, t^* is the attenuation factor, and $\ln A$ is the ln amplitude. Alternatively, the velocity v could be used instead of the slowness, where $\delta u \approx -v^{-2}\delta v$.

For the causal, constant-Q model with frequency described above, the imaginary part of the phase term is $i\omega T_R = i\omega(T - t^* \ln(\omega/\omega_r)/\pi)$, where T and t^* are both computed using the slowness at the reference frequency ω_r. The second term inside the large parentheses is the dispersion effect at different frequencies. For $\omega < \omega_r$ the dispersion results in a phase delay, and for frequencies greater than the reference frequency, a phase advance. Linearizing the dispersion term with respect to frequency for a specified frequency ω_0 results in the approximation $i\omega[T - t^*(1 + \ln(\omega_0/\omega_r)/\pi] + i\omega_0 t^*/\pi$, where the first term is the time shift for the pulse and the last term is a pulse phase distortion. This is similar to the results of Červený & Frangie (1980, 1982) for a Gabor wavelet, where they specify ω_0 as the dominant frequency of the attenuated Gabor pulse and use ω_r as the frequency at which the attenuation model is referenced. The sensitivity of the real part of the traveltime T_R, including dispersion effects, is then

$$\frac{\partial T_R}{\partial u} = \frac{\partial T}{\partial u} - \frac{\partial t^*}{\partial u}[1 + \ln(\omega_0/\omega_r)]/\pi,$$

$$\frac{\partial T_R}{\partial Q^{-1}} = -\frac{\partial t^*}{\partial Q^{-1}}[1 + \ln(\omega_0/\omega_r)]/\pi, \quad (12)$$

where ω_r specifies the reference frequency at which the

attenuation model is referenced, and ω_0 is the frequency value for the linearization of the phase-dispersion term. Here we use the estimated instantaneous frequency of the observed pulse for ω_0. We then obtain the partial derivative of T and t^* from δT and δt^* given by (7) and (10) above.

The amplitude data are normalized to the amplitude of the reference pulse for a near-offset receiver. The amplitude partials can then be written as

$$\frac{\partial \ln A}{\partial u} = \frac{\partial \ln A_g}{\partial u} + \frac{\partial \ln A}{\partial t^*}\frac{\partial t^*}{\partial u}, \qquad \frac{\partial \ln A}{\partial Q^{-1}} = \frac{\partial \ln A}{\partial t^*}\frac{\partial t^*}{\partial Q^{-1}}, \tag{13}$$

where A_g is the geometric spreading component of the amplitude related to the slowness or velocity model.

Reciprocity places important constraints on the data analysis and the inversion of seismic attributes. Spatial reciprocity aids in picking traveltimes since $T(x_2, x_1) = T(x_1, x_2)$. In this relation, the receiver location is the first argument and the source location is the second. The attenuation factor $t^* = \int u Q^{-1}\, ds$ also exhibits spatial reciprocity, $t^*(x_2, x_1) = t^*(x_1, x_2)$. However, for attenuation values, typically only relative t^* values are measured. This relative attenuation can be written as $t^*(x; x_{\text{ref}}, x_0) = t^*(x, x_0) - t^*(x_{\text{ref}}, x_0)$, where $t^*(x_{\text{ref}}, x_0)$ is the attenuation factor of the reference pulse for x_{ref} near the source location x_0. Assuming multiple sources and receivers with sufficient reciprocal points, the near-offset attenuation factors can be estimated using reciprocity. Reciprocity constraints also yield more consistent data residuals for inversion.

Fig. 5(a) is an example from the Ouachita PASSCAL experiment of the use of reciprocity to estimate the initial t^* values of the near-offset traces. In Fig. 5(a), the t^* values are plotted at the midpoint between source and receiver to compare reciprocity between shot gathers better. For comparison with initial traveltimes in Fig. 5(b), the t^* values in Fig. 5(a) start at a constant half-offset of 1 km reference distance. Since there are multiply crossing branches, a small preliminary inverse problem can be set up to determine the near-offset t^* values using reciprocity between shot gathers. At one seismic gather, the near-offset t^* value must be estimated based on the relative initial t^* values of the gather. The absolute t^* values can then be estimated by incorporating the near-offset reference station t^* values obtained from matching reciprocity.

The t^* values displayed in Fig. 5(a) are consistent with the inversion results of Lutter, Nowack & Braile (1990) who show that the subsurface structure in this region includes a shallow basin deepening to the south. This can be seen in the initial traveltimes for 2 km offset (Fig. 5b). Since the t^* values include both velocity and attenuation, the initial reference values of t^* should also show this velocity-induced variation. If it is not possible to estimate the near-offset t^* values, relative t^* values can also be used for inversion. For example, relative t^* values have been used by Matheney, Nowack & Trehu (1996) for refraction data recorded in the Lake Superior region because of the lack of reciprocity points. In either case, relative amplitudes must be used since initial source strengths are unknown.

A damped inversion can then be used to solve (11). At the nth iteration,

$$\mathbf{d} - \mathbf{g}(\mathbf{x}_n) = \mathbf{G}_n(\mathbf{x} - \mathbf{x}_n), \tag{14}$$

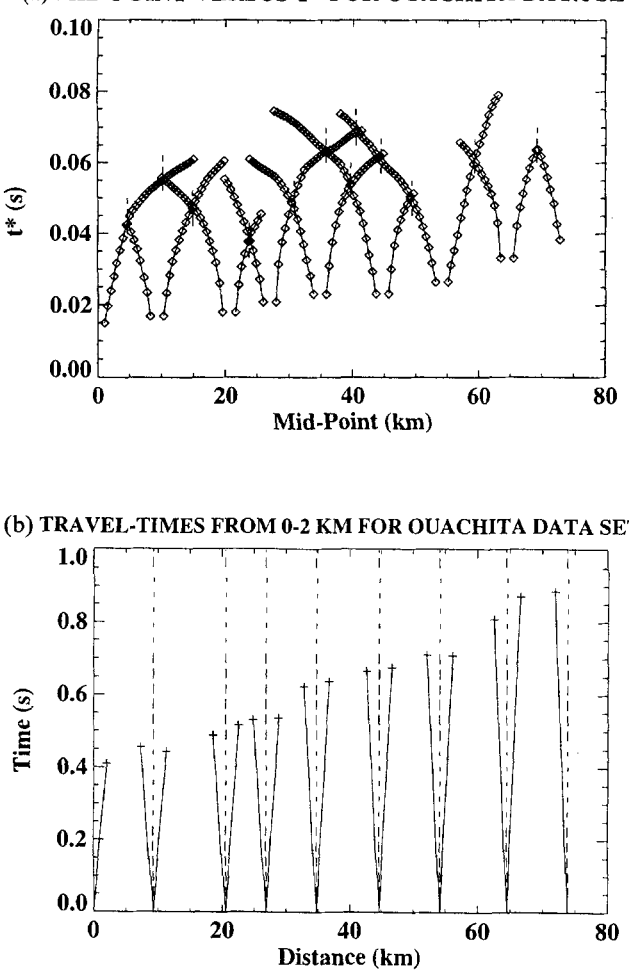

Figure 5. (a) t^* values from the Ouachita PASSCAL experiment plotted at the midpoint between source and receiver points. The dashed vertical lines show the reciprocal distances where the t^* values for two shot gathers cross. For comparison with (b), the initial t^* values are shown at a constant starting midpoint of 1 km instead of the variable initial distances of the nearby reference stations. (b) Near-offset traveltime values varying linearly from 0 to 2 km in offset showing the slowing of the near-surface velocities with distance to the south.

where $\mathbf{d}$ is the data vector that includes the different seismic attributes, $\mathbf{g}(\mathbf{x}_n)$ is the solution to the forward problem using the nth iteration model $\mathbf{x}_n$, and $\mathbf{G}_n = \partial \mathbf{g}(\mathbf{x}_n)/\partial \mathbf{x}$ is the sensitivity matrix. The data-residual vector can be normalized as $\mathbf{d}' = \mathbf{C}_d^{-1/2}[\mathbf{d} - \mathbf{g}(\mathbf{x}_n)]$ where $\mathbf{C}_d$ is the estimated data covariance matrix. It is assumed that the data are uncorrelated and, therefore, that the data covariance matrix is diagonal. This weighting is used to equalize the residuals for the different data attributes. The model residuals can also be normalized using a weighting $\mathbf{x}' = \mathbf{C}_{x_n}^{-1/2}(\mathbf{x} - \mathbf{x}_n)$, where $\mathbf{C}_{x_n}$ is the weighting matrix. For a stochastic inversion, $\mathbf{C}_{x_n}$ can be interpreted as an *a priori* model covariance matrix (Tarantola 1987) which restricts the movement of the solution at each iteration.

Using the normalizations above, the nth iteration can be written as $\mathbf{d}' = \mathbf{G}_n'\mathbf{x}'$ where $\mathbf{G}_n' = \mathbf{C}_d^{-1/2}\mathbf{G}_n\mathbf{C}_{x_n}^{1/2}$. The updated solution is then obtained by minimizing $(\mathbf{d}' - \mathbf{G}_n'\mathbf{x}')^{\mathrm{T}}(\mathbf{d}' - \mathbf{G}_n'\mathbf{x}') + \mathbf{x}'^{\mathrm{T}}\mathbf{x}'$, where T represents the conjugate transpose. The solution is of

the form

$$\mathbf{x}' = (\mathbf{G}_n'^{\mathrm{T}}\mathbf{G}_n' + \mathbf{I})^{-1}\mathbf{G}_n'^{\mathrm{T}}\mathbf{d}', \tag{15}$$

where the damping is now an identity and the updated solution can be written $\mathbf{x} = \mathbf{x}_n + \mathbf{C}_{x_n}^{1/2}\mathbf{x}'$. Iterative inversion techniques (Paige & Saunders 1982) are used to solve (15). The solution is a damped, iterative inversion rather than a more formal stochastic inversion because, in the procedure followed here, the model parametrization can change at each iteration. This choice allows for a small number of model parameters in the early iterations representing a smooth model, and an increasing number of model parameters at later iterations. The iterative procedure is terminated when the data residuals are within the estimated data uncertainties. At that point, no further refinement in the model is warranted by the data. An estimate of the uncertainties in the model parameters can be obtained from $\mathbf{C}_x = \langle \Delta\mathbf{x}\Delta\mathbf{x}^{\mathrm{T}} \rangle = \mathbf{C}_{x_n}^{1/2}\mathbf{C}_{x'}\mathbf{C}_{x_n}^{1/2}$, where $\mathbf{C}_{x'} = (\mathbf{G}_n'^{\mathrm{T}}\mathbf{G}_n' + \mathbf{I})^{-1}$ is obtained from the final iteration.

In the procedure described above, a sequence of linearized inversion is performed from smooth to less smooth models by increasing the number of model parameters at each iteration step. This procedure has the advantage of determining the longer-wavelength features of the model early in the inversion, hence explaining as much of the data as possible by a smooth, broad structure. If smooth interpolations are used, such as by splines, the procedure provides damping for each iteration, as well as smoothing of the final solution.

In order to test the method, an inversion of synthetic data was performed. The locations of the seismic profiles are the same as the observed data example below. The true model used for the test inversion is a basin structure with lower velocity and Q (Fig. 6a). The starting model is a 1-D model similar to the left edge of the velocity and attenuation models in Fig. 6(a). The traveltimes, ln amplitudes and t^* values are shown in Fig. 6(b), where the solid lines are from the starting 1-D model and the plus signs are from the true model. An iterative AFT inversion was perfomed progressing from three to five and finally to nine vertical node lines. The final inverted velocity and attenuation models are shown in Fig. 7(a), and are very similar to the true models shown in Fig. 6(a). The

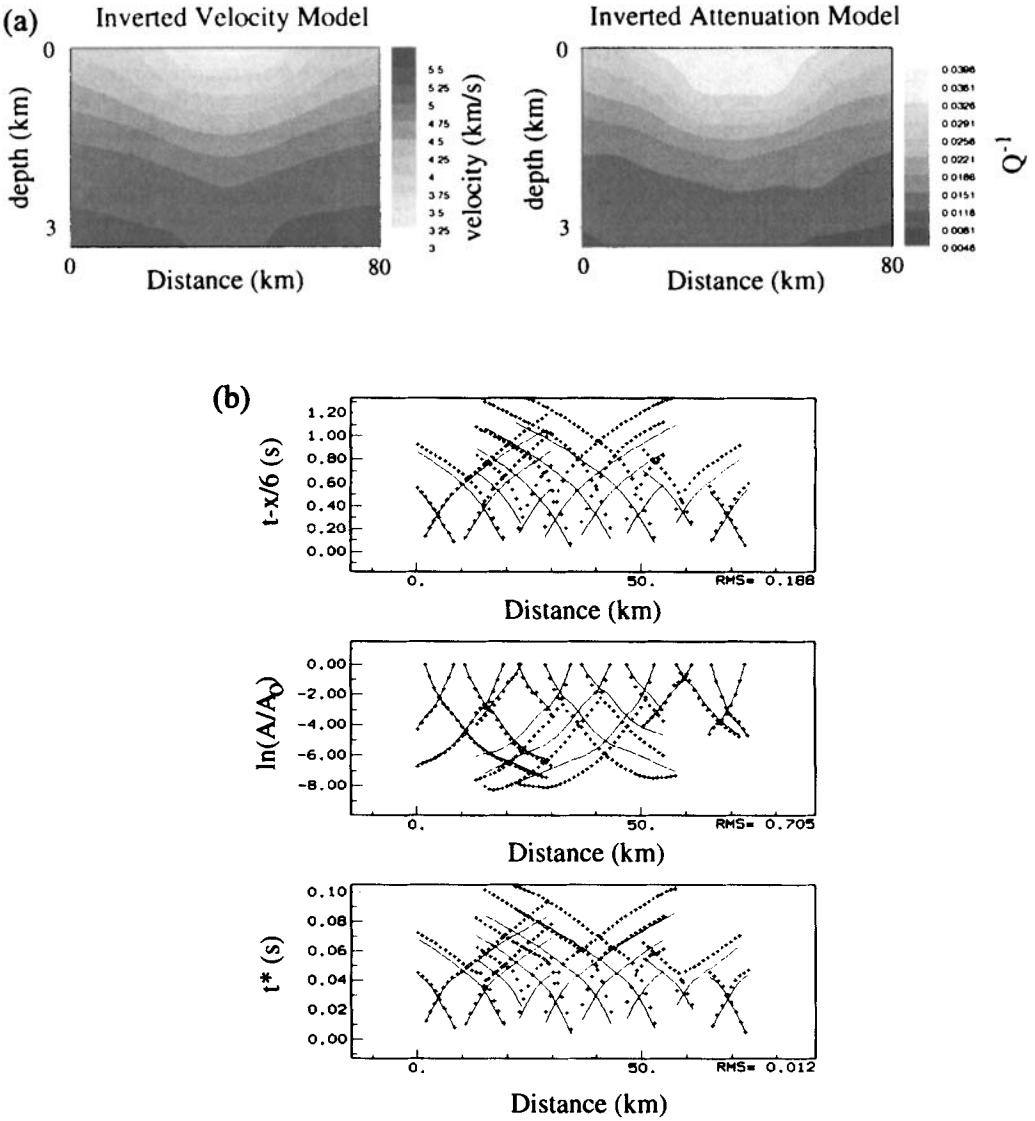

Figure 6. (a) The true velocity and attenuation models used for a test inversion. (b) The traveltimes, ln amplitudes and t^* values from the starting 1-D model (solid lines) and the true model (plus signs).

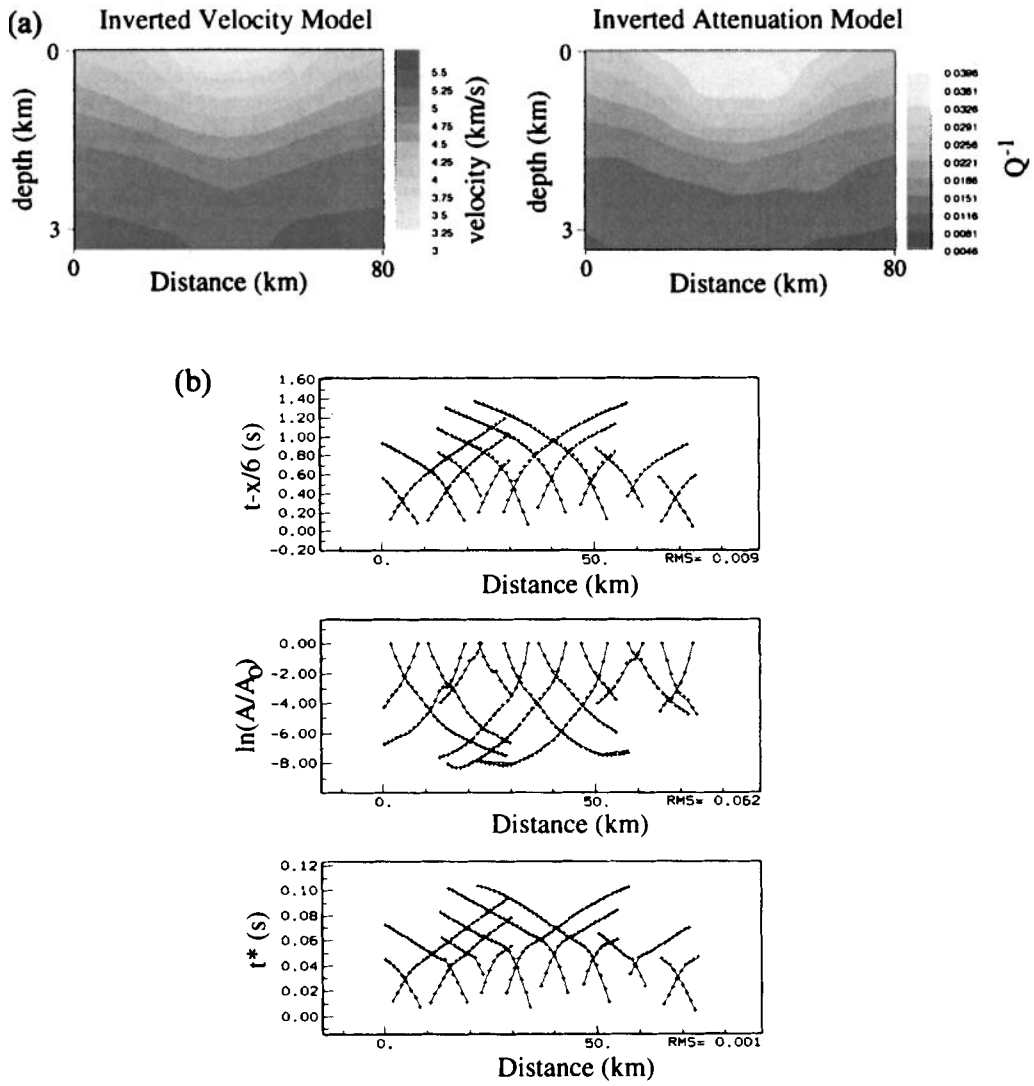

Figure 7. (a) The inverted velocity and attenuation models from the AFT inversion. (b) The traveltimes, ln amplitudes and t^* values from the final inverted model (solid lines) and the true model (plus signs).

only deviations from the true model are at greater depths for ranges larger than 50 km where the attribute data are more limited in offset. An excellent fit is shown in Fig. 7(b) between the data computed from the inverted model (solid lines) and from the true model (plus signs). This example shows that the iterative AFT inversion can reconstruct the subsurface model for the given source and receiver geometry.

APPLICATION TO THE OUACHITA PASSCAL EXPERIMENT

To illustrate the AFT inversion, we inverted for shallow crustal structure along the northern end of the array of the PASSCAL Ouachita seismic experiment. We iterated from smooth to less smooth models by increasing the number of vertical node lines in the model at each iteration step. We used a starting model derived from forward modelling of one of the central data profiles. The model had five vertical nodes at depths of 0.0, 0.75, 1.5, 2.25 and 3.25 km. The iteration sequence began with two vertical node lines and then progressed to three, five, and finally nine equally spaced vertical node lines between 0 and 80 km. The resulting final model with nine vertical node lines had 45 velocity and 45 attenuation nodes. The iterative process was terminated as described above. This iterative, progressively detailing process was found to be essential when performing simultaneous inversions of more than one seismic attribute. In particular, amplitudes were found to be very sensitive to model roughness, and smooth preliminary models were needed to avoid local minima in the solution.

The final velocity model with nine vertical node lines is shown in Fig. 8(a) and includes a shallow basin deepening to the south. This basin is also imaged in the attenuation Q model (Fig. 8b). The attenuation model has Q values as low as 20 near the surface, increasing to greater than 100 for depths near 3 km. Fig. 9(a) shows the ray diagram for the final crustal model shown in Fig. 8. Fig. 9(b) shows a comparison between the observed and computed traveltimes, and Figs 9(c) and (d) show the observed and predicted ln amplitudes and t^* values. For the final iteration with nine vertical node lines, RMS residuals were within the estimated

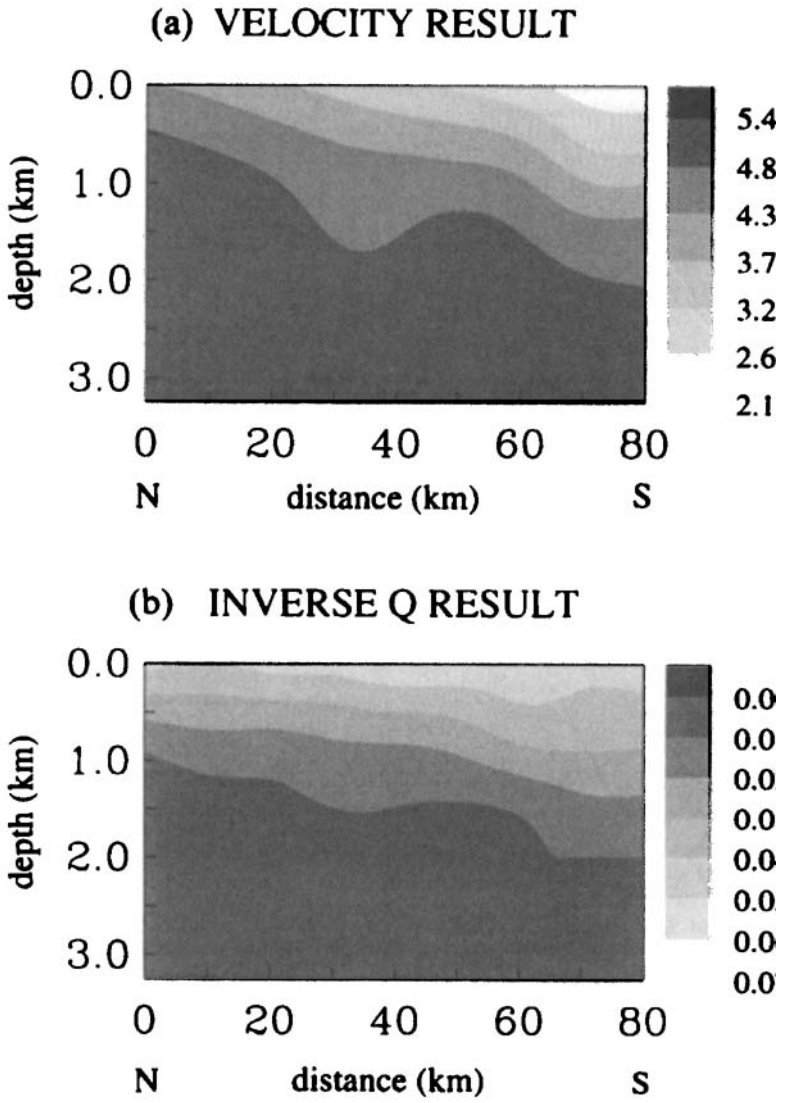

Figure 8. Iterative inversion of seismic attributes for refraction data from the Ouachita PASSCAL experiment using 45 model nodes. (a) Inverted velocity model. (b) Inverted Q^{-1} attenuation model.

data errors for all the seismic attributes so no further refinement of the model was made.

Approximate estimates of the model errors were obtained from the model covariance matrix at the final iteration. Since the node spacing was somewhat variable in depth, the error estimates were scaled prior to plotting to equalize the effect of relative area between the nodes approximately. A scaling of the variances by this area is used to display the errors. Although the area under the splines is a better estimate, we found that the node spacings gives an adequate relative area estimate. This normalization is similar to the relative scaling of variances for variable block size described by Nolet (1987). In that approach, the prior variances, which also determine the initial damping, are scaled by the volume between the nodes. However, in our example a variable node spacing in depth was chosen to account for fewer rays at depth. Fig. 10(a) shows the scaled model errors for velocity and Fig. 10(b) for inverse Q.

The cross-correlation between velocity and inverse Q for each node was estimated from the corresponding off-diagonal elements of the covariance matrix. The cross-correlations were found to be in the range -0.12 to 0.0, indicating that the velocity and inverse-Q values are being resolved from one another with a slight negative correlation.

A comparison between the observed ln amplitudes and the predicted part of the amplitudes due to geometric spreading is shown in Fig. 11, which shows that approximately half of the predicted ln amplitudes from this model resulted from geometric spreading and the rest from the attenuation model. This result is similar to observations using reflection-seismic data, where amplitude gain corrections require both geometric spreading and attenuation factors (Claerbout 1985).

The seismic amplitudes in the inversion were found to be very sensitive to model roughness. This sensitivity of ray amplitudes was noted by Nowack & Lutter (1988), who suggested that geometric amplitudes could be used to resolve small-scale features better than traveltimes alone. This was also noted by Neele, Van Decar & Snieder (1993). However, from the observed crustal data used here, relatively smooth inverted models were required to match the observed

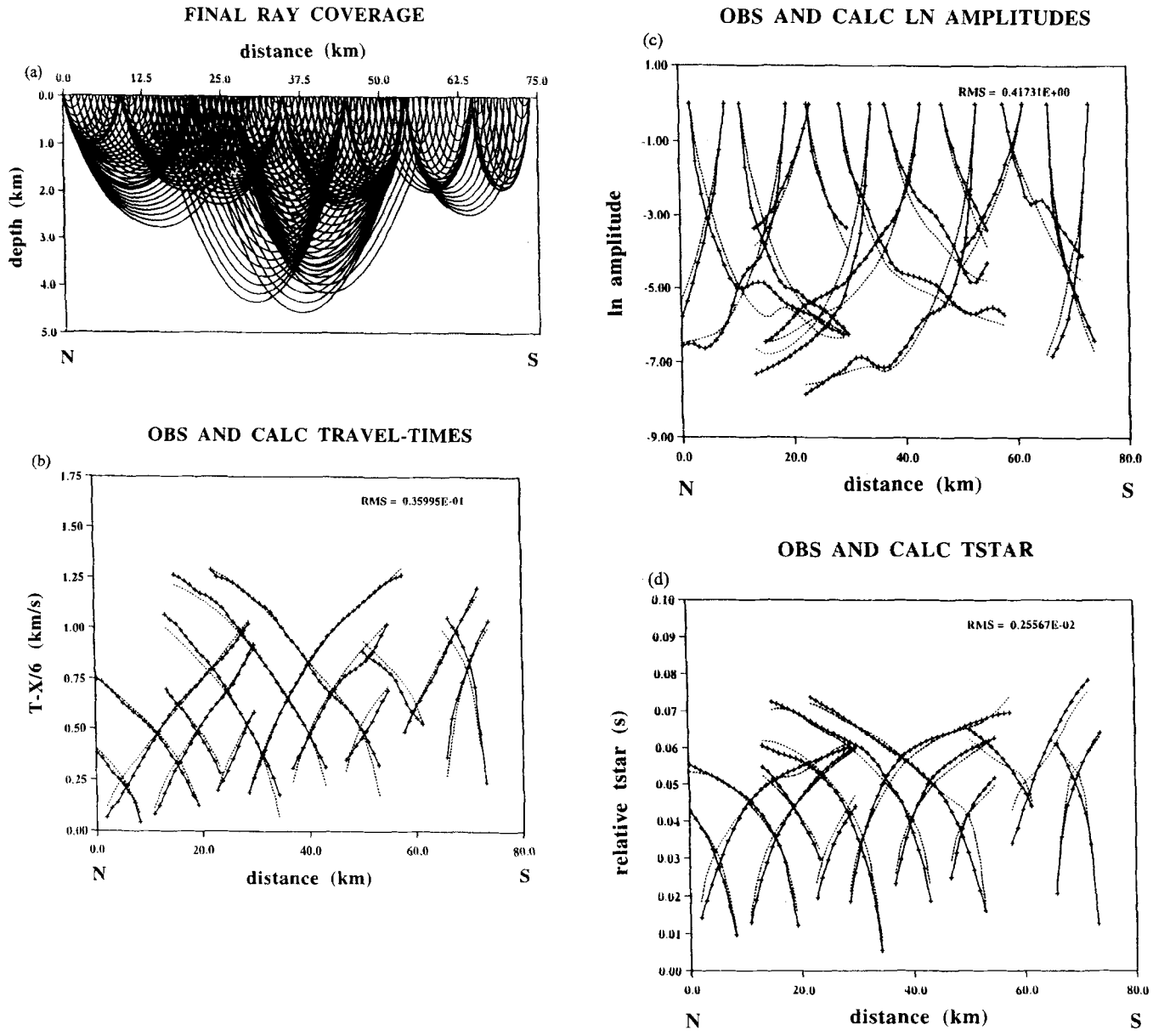

Figure 9. (a) The ray diagram for the crustal model shown in Fig. 8. (b) Observed and computed traveltimes for the crustal model shown in Fig. 8. (c) Observed and predicted ln amplitudes. (d) Observed and predicted t^* values. The RMS residuals are shown in the upper right for each data attribute. For each attribute, the observed data is shown with crosses and the predicted data by dashed lines.

amplitudes and t^* data. To maintain a smooth solution required that an iterative procedure from smooth to less smooth models be performed. Also, including amplitudes and t^* values at each step of the inversion was required in order to fit all the seismic attributes at the final iteration.

CONCLUSIONS

We have developed a simultaneous inversion for seismic attributes, referred to as AFT inversion for amplitude, instantaneous frequency, and traveltime. AFT inversion includes more of the seismic data than just traveltimes, but has less sensitivity to noise than complete wavefield inversions. Instantaneous frequencies are converted to attenuation factors, t^*, using a matching procedure between the data and near-offset reference pulses. This procedure approximately compensates for the effects of the source spectra in the estimation of the attenuation factors.

For inversion, ray-perturbation methods are used to compute the sensitivity of the different attributes to variations in the model. Only first-order perturbations of the seismic attributes with respect to the model parameters are used at each iteration, so as to keep the order of perturbation the same at each iteration. Higher-order perturbations of the seismic attributes are incorporated by using multiple iterations.

An iterative inversion is then performed starting with smooth models (few nodes) and progressing to less smooth models (many nodes). This procedure was found to be important when simultaneously inverting different seismic attributes. The AFT inversion is terminated when the RMS residuals are within the data errors.

To illustrate the AFT inversion for laterally varying

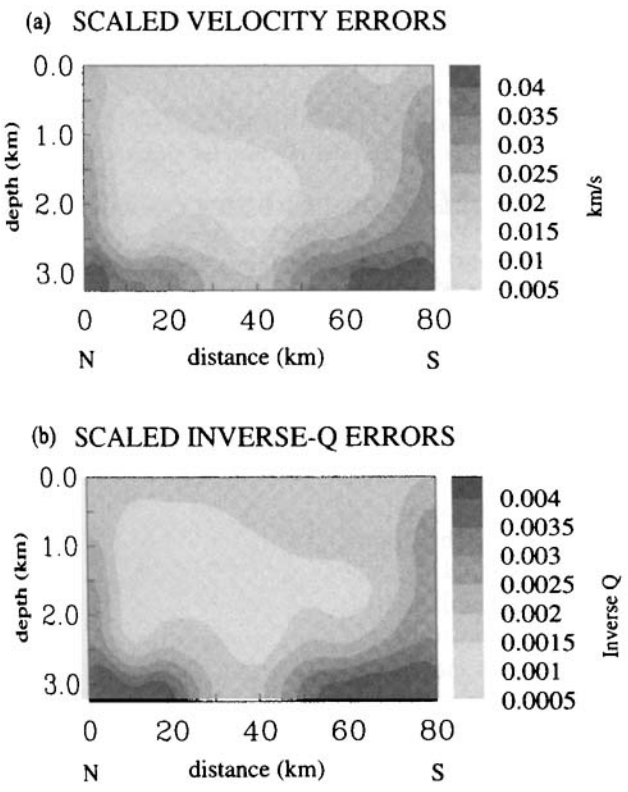

Figure 10. The scaled errors for (a) velocity and (b) inverse Q for the inversion model in Fig. 9. In (a) and (b), the variances are scaled by areas represented by the node spacing.

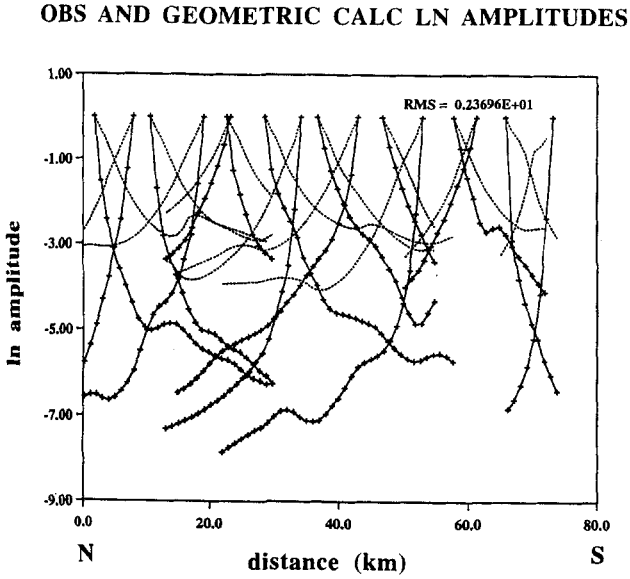

Figure 11. A comparison between the observed ln amplitudes (solid lines with plus signs) and the computed ln amplitudes resulting from just geometric spreading (dashed lines). Here, about half of the observed ln amplitudes are explained by the velocity model and the rest by the attenuation model.

structure, observed crustal refraction data from the Ouachita PASSCAL experiment have been used to invert for shallow crustal structure. Although the amplitude data is sensitive to model roughness, the inverted velocity and attenuation models were required by the data to maintain a relatively smooth character. Also, the amplitude and t^* data were needed, along with the traveltimes, at each step of the inversion to ensure that all the seismic attributes were fitted at the final iteration.

REFERENCES

Aki, K. & Richards, P.G., 1980. *Quantitative Seismology Theory and Methods,* W.H. Freeman, San Francisco, CA.

Červený, V., 1985. Gaussian beam synthetic seismograms, *J. Geophys.,* **58,** 44–72.

Červený, V. & Frangie, A., 1980. Elementary seismograms of seismic body waves in dissipative media, *Studia Geoph. Geod.,* **24,** 365–372.

Červený, V. & Frangie, A., 1982. Effects of causal absorption on seismic body waves, *Studia Geoph. Geod.,* **26,** 239–253.

Červený, V. & Hron, F., 1980. The ray series method and dynamic ray tracing system for 3-D inhomogeneous media, *Bull. seism. Soc. Am.,* **70,** 47–77.

Červený, V., Popov, M.M. & Pšenčík, I., 1982. Computations of wavefields in inhomogeneous media—Gaussian beam approach, *Geophys. J. R. astr. Soc.,* **70,** 109–128.

Chapman, C.H. & Drummond, R., 1982. Body-wave seismograms in inhomogeneous media using Maslov asymptotic theory, *Bull. seism. Soc. Am.,* **72,** S277–S317.

Claerbout, J.F., 1985. *Imaging the Earth's Interior,* Blackwell Scientific Publications, Oxford.

Cohen, L., 1985. *Time–Frequency Analysis,* Prentice-Hall, Englewood Cliffs, NJ.

Daubechies, I., 1992. *Ten Lectures on Wavelets,* Society of Industrial and Applied Mathematics, Philadelphia, PA.

Farra, V. & Madariaga, R., 1987. Seismic waveform modeling in heterogeneous media by ray perturbation theory, *Geophys. J. R. astr. Soc.,* **92,** 2697–2712.

Farra, V., Virieux, J. & Madariaga, R., 1989. Ray perturbation theory for interfaces, *Geophys. J. Int.,* **99,** 377–390.

Farra, V., Madariaga, R. & Virieux, J., 1994. Comment on 'The ambiguity in ray perturbation theory' by Roel Sneider and Malcolm Sambridge, *J. geophys. Res.,* **99,** 21 963–21 968.

Hu, G. & Menke, W., 1992. Formal inversion of laterally heterogeneous velocity structure from P-wave polarization data, *Geophys. J. Int.,* **110,** 63–69.

Keller, J.B., 1962. Wave propagation in random media *Proc. Symp. appl. Math.,* **13,** 227–246.

Lutter, W.J., Nowack, R.L. & Braile, L.W., 1990. Seismic imaging of upper crustal structure using travel times from the PASSCAL Ouachita experiment, *J. geophys. Res.,* **95,** 4621–4631.

Matheney, M.P. & Nowack, R.L., 1995. Seismic attenuation values obtained from instantaneous frequency matching and spectral ratios, *Geophys. J. Int.,* **123,** 1–15.

Matheney, M.P., Nowack, R.L. & Trehu, A.M., 1996. Seismic attribute inversion for velocity and attenuation structure using data from the Glimpce Lake Superior experiment, *J. geophys. Res.,* submitted.

Moore, B.J., 1980. Seismic ray theory for lithospheric structures with slight lateral variations, *Geophys. J. R. astr. Soc.,* **63,** 671–689.

Moore, B.J., 1991. Seismic rays in media with slight lateral variations in velocity, *Geophys. J. Int.,* **105,** 213–227.

Neele, F., Van Decar, J. & Snieder, R., 1993. The use of P wave amplitude data in a joint inversion with travel times for upper mantle velocity structure, *J. geophys. Res.,* **98,** 12 033–12 054.

Nolet, G., 1987. Seismic wave propagation and seismic tomography, in *Seismic Tomography,* pp. 1–24, ed. Nolet, G., Reidel, Dordrecht, the Netherlands.

Norton, S.J. & Linzer, M., 1982. Correcting for ray refraction in velocity and attenuation tomography: a perturbation approach, *Ultrason. Imag.,* **4,** 201–233.

Nowack, R.L. & Aki, K., 1984. The 2-D Gaussian beam synthetic method: testing and application, *J. geophys. Res.,* **89,** 7797–7819.

Nowack, R.L. & Lutter, W.J., 1988. Linearized rays, amplitude and inversion, *Pure appl. Geophys.*, **128,** 401–421.

Nowack, R.L. & Lyslo, J.A., 1989. Fréchet derivatives for curved interfaces in the ray approximation, *Geophys. J. Int.*, **97,** 497–509.

Paige, C.C. & Saunders, M.A., 1982. LSQR: an algorithm for sparse linear equations and sparse least squares, *Assn. Comp. Mach. Trans. Math. Software,* **8,** 43–71.

Popov, M.M. & Pšencík, I., 1978. Computation of ray amplitudes in inhomogeneous media with curved interfaces, *Studia Geophys. Geol.,* **22,** 248–258.

Snieder, R. & Aldridge, D.F., 1995. Perturbation theory for travel times, *J. acoust. Soc. Am.,* **98,** 1565–1569.

Snieder, R. & Sambridge, M., 1992. Ray perturbation theory for traveltimes and ray paths in 3-D heterogeneous media, *Geophys. J. Int.,* **109,** 294–322.

Snieder, R. & Sambridge, M., 1993. The ambiguity of ray perturbation theory, *J. geophys. Res.,* **98,** 22 021–22 034.

Snieder, R. & Spencer, C., 1993. A unified approach to ray bending, ray perturbation and paraxial ray theories, *Geophys. J. Int.,* **115,** 456–470.

Taner, M.T., Koehler, F. & Sheriff, R.E., 1979. Complex seismic trace analysis, *Geophysics,* **44,** 1041–1063.

Tarantola, A., 1987. *Inverse Problem Theory,* Elsevier, Amsterdam.

Zhu, T. & Chun, K.-Y., 1994. Complex rays in elastic and anelastic media, *Geophys. J. Int.,* **118,** 181–193.